Iranian Journal of Materials Forming 14 (1) (2027) 37-54

IJMF

Online ISSN: 2383-0042

Iranian Journal of Materials Forming

Journal Homepage: http://ijmf.shirazu.ac.ir

Research Article

Influence of Joint Angle on Residual Stress, Microstructural Evolution, and Mechanical Performance of Friction Stir Welded AA6061 Aluminum Alloy Using a Novel Adjustable Angled-Joint Fixture

Farzad AghaAbdollahian and Mohammad Honarpisheh*

Faculty of Mechanical Engineering, University of Kashan, Kashan, Iran

ARTICLE INFO

Article history:

Received: 6 April 2026
Reviewed: 16 May 2026
Revised: 12 June 2026
Accepted: 14 June 2026

Keywords:

Friction stir welding
Joint angle
Mechanical properties
Digital image correlation
Microstructural evolution

Please cite this article as:

AghaAbdollahian, F. & Honarpisheh, M. (2027). Influence of joint angle on residual stress, microstructural evolution, and mechanical performance of friction stir welded AA6061 aluminum alloy using a novel adjustable angled-joint fixture. *Iranian Journal of Materials Forming*, *14*(1), 37-54. https://doi.org/10.22099/IJMF.2026.55897.1378

ABSTRACT

Friction stir welding (FSW) is a solid-state joining technique capable of producing high-quality joints through frictional heating and severe plastic deformation below the melting point. In this study, the effect of joint angle on the residual stress evolution and integrated mechanical response of AA6061 aluminum alloy was experimentally investigated. Rolled plates (185 × 100 × 4 mm) were annealed prior to welding to improve ductility and material flow. A novel adjustable fixture enabled the fabrication of joints at 90°, 150°, 165°, and 180°, while welding was performed at 1400 rpm and 16 mm/min using angle-specific tools. Residual stresses were quantified using a hybrid digital image correlation–incremental hole drilling (DIC–IHD) method. Microstructural characterization and through-thickness microhardness measurements were conducted to elucidate thermo-mechanical behavior, and tensile tests were performed to evaluate joint performance. Increasing the joint angle progressively reduced tensile residual stresses from 189.5 and 177.3 MPa at 90° to 159.3 and 150.3 MPa at 180° in longitudinal and transverse directions, respectively. The 165° configuration exhibited the most homogeneous microstructure, uniform hardness distribution, and superior tensile strength. The results demonstrate that joint angle governs material flow symmetry and recrystallization behavior, leading to an optimal thermo-mechanical condition at 165° for enhanced structural performance.

1. Introduction

Friction stir welding (FSW) is a solid-state joining process developed by The Welding Institute (TWI) in 1991 [1], which enables high-quality joints without melting the base material [2]. By utilizing frictional heat and mechanical stirring, FSW induces intense plastic deformation, making it highly effective for aluminum alloys—materials that often suffer from porosity and hot cracking in fusion welding [3]. Due to these advantages,

* Corresponding author
E-mail address: honarpishe@kashanu.ac.ir (M. Honarpisheh)
https://doi.org/10.22099/IJMF.2026.55897.1378

including low distortion and high dimensional stability, FSW is widely adopted in the aerospace, automotive, and shipbuilding industries [4].

Fig. 1 illustrates the FSW process, where a non-consumable rotating tool—featuring a specifically designed shoulder and pin—is plunged into the workpiece and traversed along the joint line. The generated frictional heat promotes intense plastic deformation and solid-state bonding, forming the joint through the advancing, retreating, and nugget zones [2]. Friction stir welding has emerged as a robust solid-state joining technique for aluminum alloys, offering superior mechanical properties and minimal defect formation compared to conventional fusion welding. The tensile performance of FSW joints has been extensively investigated in recent years. Beygi et al. [5] examined the influence of tool geometry and process parameters on the tensile strength of AA2024–AA7075 dissimilar joints, highlighting the critical role of the pin profile in enhancing joint integrity. Similarly, Prodkornburee et al. [6] employed coupled Eulerian–Lagrangian simulations to model the tensile response of dissimilar aluminum welds, demonstrating the influence of material flow patterns on fracture behavior. Thilagham et al. [7] optimized process parameters for AA7075–AA6082 joints using response surface methodology, revealing a strong correlation between heat input and ultimate tensile strength. Residual stresses, which play a decisive role in determining fatigue performance, dimensional stability, and post-weld distortion of FSW joints, have also been extensively investigated. Garcia Ruano et al. [8] quantified residual stresses in AA5052 welds using the acoustoelasticity technique, while Vahidshad et al. [9] conducted finite element modeling to predict stress evolution under various thermal conditions. Wiley et al. [10] analyzed the correlation between fatigue life and residual stress distribution in double-sided FSW joints, emphasizing the role of weld symmetry in stress balancing. In addition, several researchers have employed advanced hybrid methods such as Digital Image Correlation (DIC), hole-drilling, and neutron diffraction to experimentally characterize residual stress fields with high spatial resolution [11, 12]. These

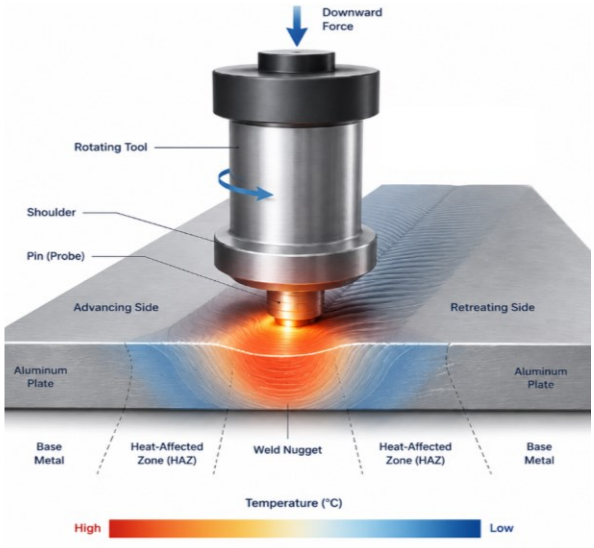

Fig. 1. Schematic representation of the FSW process.

approaches have collectively improved the understanding of the thermo-mechanical behavior of FSW joints under complex stress states. The thermal–mechanical impact of tool geometry has been another focal point of recent studies. Manikandan et al. [13] examined various pin profiles in AA6061-T6 and AA7075-T6, concluding that tapered tools improve heat distribution and minimize defect formation. Similarly, Zhang et al. [14] investigated Cu–Al dissimilar joints, reporting that the shoulder structure significantly governs temperature gradients and grain refinement. Regarding joint configuration, several researchers have explored non- linear geometries and hybrid designs. Beygi et al. [15] introduced a hybrid lap–butt configuration for aluminum-to-steel FSW tee joints, achieving enhanced tensile strength and improved microstructural homogeneity. Ahmed et al. [16] investigated T-joints between AA2024-T4 and AA7075-T6 alloys, highlighting the effect of tool offset on weld quality. Jesus et al. [17] analyzed corner joints using pre-set wires and progressive pin profiles, demonstrating improved bonding and reduced interfacial defects. Despite the considerable progress achieved in understanding the influence of process parameters, tool geometry, and heat generation on the quality of friction stir welded joints, the effect of joint configuration—particularly the joint angle—on the thermo- mechanical response and residual stress evolution of aluminum welds remains largely unexplored. Most previous investigations have been confined to conventional butt and lap joints, providing limited insight into the complex stress distribution and strength characteristics associated with angled or non-linear joints frequently encountered in practical applications. In addition, prior numerical – experimental studies on dissimilar friction stir welding [18] (e.g., AA5086–AA6061) have combined three-dimensional thermo-mechanical finite element modeling with hole-drilling residual-stress measurements, showing that tool rotational speed markedly affects the maximum tensile residual stress, traverse speed mainly influences the distribution of transverse residual stresses, and fixture conditions can significantly alter both the magnitude and distribution of residual stresses. These findings underscore the importance of reliable residual-stress characterization when assessing and optimizing FSW joints.

In this context, the present study experimentally examines the effect of different joint angles (90°, 150°, 165°, and 180°) on the residual stress distribution and mechanical performance of AA6061 aluminum alloy joints produced by friction stir welding. The selected joint angles were defined as representative experimental configurations to comparatively evaluate the influence of joint geometry on the welding response. To enable accurate control of the joint configuration, a novel adjustable fixture was designed, and dedicated tools were fabricated for each joint angle configuration. Residual stresses were measured using the hybrid digital image correlation–incremental hole drilling (DIC–IHD) method, while tensile tests were conducted to evaluate the mechanical integrity of the welds. The outcomes of this research are expected to provide a deeper understanding of how joint angle governs the thermo-mechanical behavior of friction stir welded structures, thereby contributing to the optimization of design strategies for advanced aluminum assemblies.

2. Experimental Procedure

2.1. Materials and sample preparation

The base material used in this study was aluminum alloy AA6061 in the form of rolled plates with dimensions of 185 × 100 × 4 mm. Before welding, all plates were annealed within the standard permissible temperature range for AA6061 and held isothermally for 1 h [19]. After annealing, the specimens were allowed to cool slowly inside the furnace until reaching room temperature to ensure a uniform microstructure and minimize initial residual stresses. To guarantee intimate contact along the joint line, the faying surfaces were carefully machined and successively polished so that the plates were in intimate contact and no inter-plate gap remained throughout the entire seam. According to the geometry shown in Fig. 2 and the edge configurations summarized in Table 1, the edge preparation varied depending on the target joint angle:

- 90° and 180°: square edges without bevel were used.
- 150°: a 30° bevel was introduced on the mating edges.
- 165°: a 15° bevel was introduced on the mating edges.

These configurations ensured proper alignment and consistent material flow during the friction stir welding process.

Table 1. Joint angle and bevel angle (α) for the specimens

Joint angle (°)	α (°)
90	0
150	30
165	15
180	0

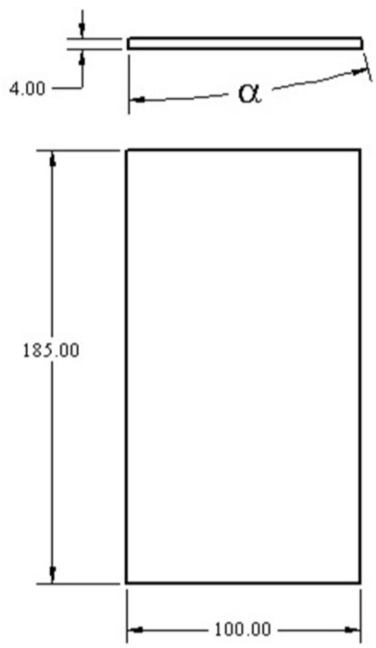

Fig. 2. Geometry of the AA6061 plates used in the experiments. Base plate dimensions: 185mm×100mm×4mm.

2.2. Fixture and joint configuration

A custom-designed steel fixture was developed to enable friction stir welding at various joint angles ranging from 90° to 180°. The fixture was fabricated by welding together steel plates with thicknesses of 8, 10, and 12 mm. To ensure adequate rigidity and prevent deformation or structural failure under the substantial axial and transverse forces generated during FSW, all regions susceptible to stress concentration were reinforced with stiffeners. Fig. 3(a) shows that the fixture consisted of five primary components:

1- A workpiece support platform serving as the seating surface for the aluminum plates,

2- A hinge assembly allowing rotation of the platform to achieve the desired joint angle,

3- An angle-adjustment lever for precise control and locking of the joint configuration,

4- clamping units to restrict both longitudinal and transverse movement of the workpieces, ensuring firm fixation during welding, and

5- a rigid base plate mounted on the milling machine table to maintain overall stability and alignment during the process.

The fixture was fabricated from structural steel (ST37). Since minor misalignments could occur during the welding and assembly of the fixture components, the contact surface of the base plate (mounting area on the milling machine table) was precision-milled after fabrication to eliminate any unevenness and to ensure perfect alignment and structural integrity of the entire assembly. As shown in Fig. 3b, the adjustable fixture could be adjusted to provide joint configuration at 90°, 150°, and 165°, corresponding to the different welding conditions investigated in this study. This design provided smooth and repeatable adjustment of the joint angle through the lever mechanism while maintaining excellent stiffness and alignment accuracy. Consequently, the fixture ensured precise positioning of the joint line along the tool path for all experimental configurations. The machine-mounted setup and workpiece configuration for angle control are presented in Fig. 4.

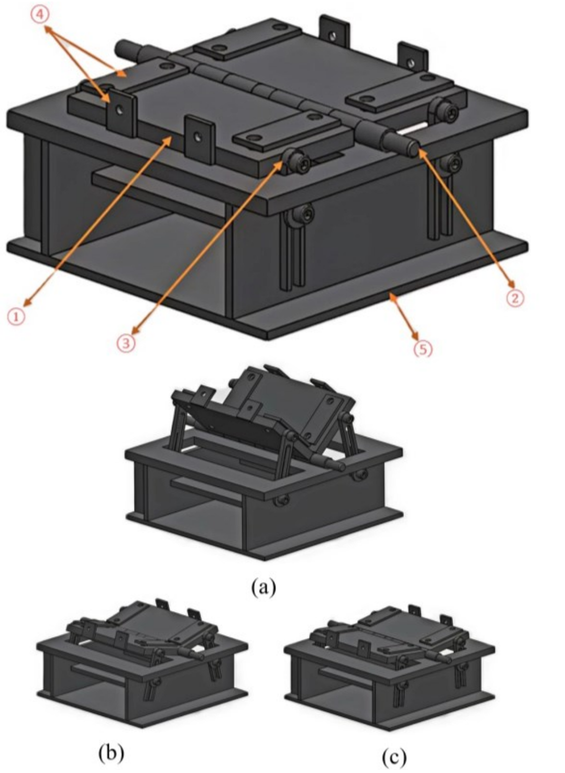

Fig. 3. Schematic of the adjustable steel fixture used in the FSW setup, illustrating its main structural components: (1) workpiece support platform, (2) hinge assembly for angular adjustment, (3) angle–adjustment lever, (4) clamping units, and (5) rigid base plate. Fixture configurations for three joint-angle setups: (a) 90°, (b) 150°, and (c) 165°.

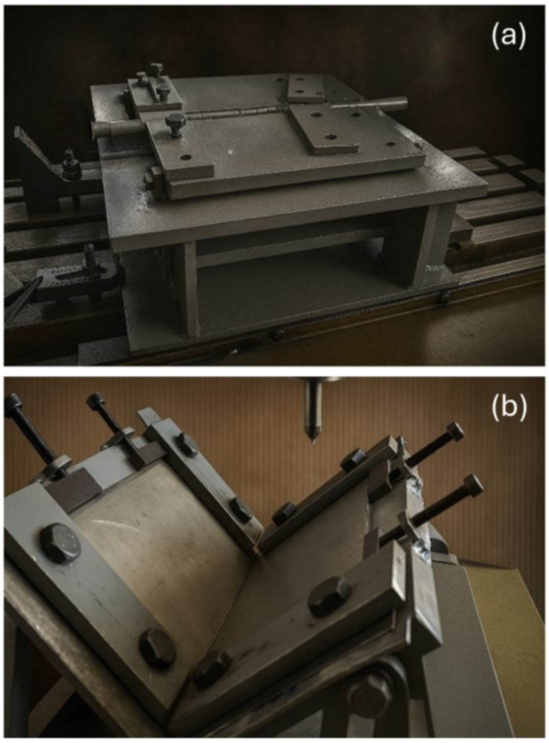

Fig. 4. Experimental photographs of the adjustable fixture: (a) machine-mounted setup and (b) workpiece configuration for angle control.

2.3. Tool design

For each joint angle (90°, 150°, 165°, and 180°), a dedicated FSW tool was designed and manufactured to ensure stable heat generation and efficient material flow consistent with the joint geometry. As illustrated in Fig. 5, four custom-built tools were prepared for the respective joint configurations. Each tool consisted of a shoulder and a conical pin without threads. The pin geometry was tapered to enhance material flow and reduce the likelihood of defect formation [20, 21], while providing sufficient stirring throughout the joint thickness. The pin length was specifically adjusted for each joint angle to guarantee proper penetration and mixing at the interface. The shoulder featured a compound geometry comprising an outer inclined region that gradually transitioned into a flat surface toward the center. This configuration facilitated smooth material consolidation, minimized flash formation, and maintained consistent heat input across all joint angles. All tools were polished to achieve a uniform surface finish, and the tool tilt angle and plunge depth were kept constant throughout the experiments to isolate the effect of joint angle on welding behavior. Table 2 summarizes the key geometric parameters of the tools employed in this study.

2.4. Welding parameters and procedure

All friction stir welding experiments were performed under identical processing conditions to ensure that any variation in the results originated solely from the joint angle. The welds were produced on a vertical milling machine (Heckert 315, Germany) operating in position-controlled mode. A constant tool rotational speed of 1400 rpm and a traverse speed of 16 mm/min were maintained for all configurations. The adjustable fixture described earlier was used to accurately set each joint angle and to securely restrain the aluminum plates against both longitudinal and transverse movement. Before each welding run, the faying surfaces and clamping interfaces were thoroughly cleaned to remove oxides and debris, ensuring consistent frictional contact and repeatable heat generation. The tool was gradually plunged into the joint line until full shoulder contact was achieved, followed by a brief dwell period to stabilize the thermal field before initiating the traverse motion. No external cooling or auxiliary heating was applied, and all welds were produced under ambient laboratory conditions. After welding, the specimens were allowed to cool naturally in still air at room temperature. Visual inspection of the weld surfaces revealed a smooth appearance and defect-free joints for all configurations. The welded joints for the four joint angles are shown in Fig. 6.

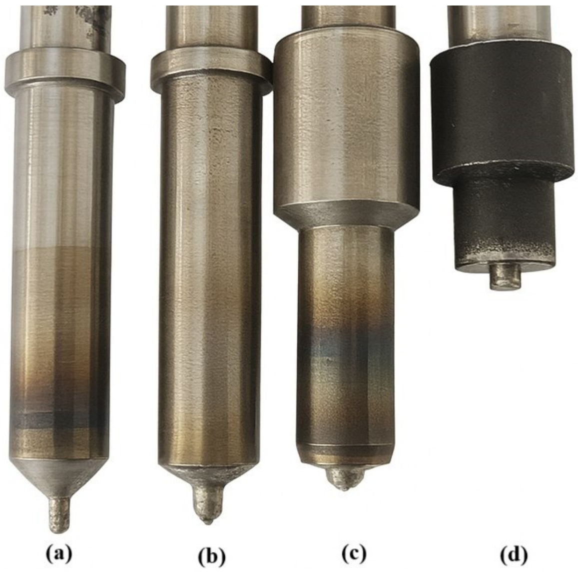

Fig. 5. Photographs of the custom-designed FSW tools used for different joint angles: (a) 90°, (b) 150°, (c) 165°, and (d) 180°.

Table 2. Geometric parameters of the FSW tools used for each joint angle

Joint angle (°)	Shoulder type	Shoulder dia.(mm)	Pin type	Pin dia. (mm, top/bottom)	Pin length (mm)
90	Inclined–flat	16	Conical	4/2	6.2
150	Inclined–flat	16	Conical	4/2	4.5
165	Inclined–flat	16	Conical	6/3	4
180	Inclined–flat	18	Conical	6/5	4

.

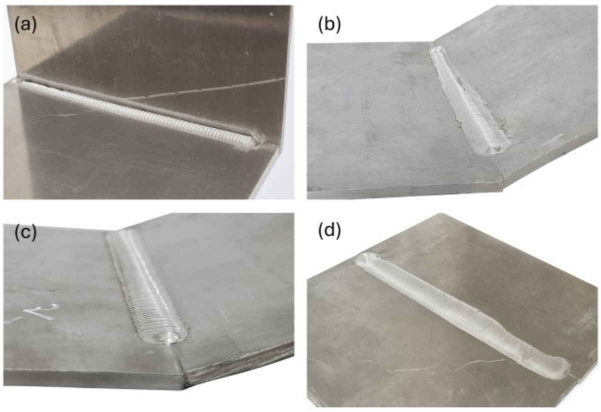

Fig. 6. Weld surfaces obtained for different joint configurations: (a) 90°, (b) 150°, (c) 165°, and (d) 180°. All joints exhibit a smooth surface appearance with no visible defects.

2.5. Residual stress measurement by the DIC–IHD method

Residual stresses in the welded joints were evaluated using a hybrid Digital Image Correlation–Incremental Hole Drilling (DIC–IHD) technique. This combined approach leverages the non-contact, full-field strain measurement capability of DIC together with the localized stress-relief principle of the IHD method, enabling accurate quantification of residual stresses in geometrically complex configurations such as angled FSW joints.

The ASTM Standard Test Method E837-13a [19] outlines the steps for this procedure. IHD represents a variant of the hole-drilling technique designed to evaluate residual stress at different depths throughout the material's thickness. As specified in ASTM E837-13a, the combined strain vectors for each group of measured strains, denoted as, ε_1 , ε_2, and ε_3 are derived using the following equations:

$$\boldsymbol{p}_i = (\varepsilon_3 + \varepsilon_1)_j/2 \tag{1}$$

$$\boldsymbol{q}_j = (\varepsilon_3 - \varepsilon_1)_j/2 \tag{2}$$

$$\boldsymbol{t}_j = (\varepsilon_3 + \varepsilon_1 - 2\varepsilon_2)_j/2 \tag{3}$$

The subscript j denotes the sequence of hole depth increments linked to the sets of measured strains ε_1 , ε_2, ε_3. For computing the residual stress, calibration matrices $\bar{a}_{jk}$ and $\bar{b}_{jk}$ are applied. These constants are available in the tables provided by the ASTM E837 standard. Using the corresponding measured strains, the residual stress at each depth increment can be determined by resolving these matrix equations:

$$(\bar{a}^T\bar{a} + \alpha_p c^T c)\boldsymbol{P} = \frac{E}{1+v}\bar{a}^T\boldsymbol{p} \tag{4}$$

$$(\bar{b}^T\bar{b} + \alpha_Q c^T c)\boldsymbol{Q} = E\bar{b}^T\boldsymbol{q} \tag{5}$$

$$(\bar{b}^T\bar{b} + \alpha_T c^T c)\boldsymbol{T} = E\bar{b}^T\boldsymbol{t} \tag{6}$$

The combined strains p, q, and t are as defined in Eqs. (1)–(3). To minimize significant errors during calculations, Tikhonov regularization based on the second derivative is applied via a tri-diagonal matrix c. The initial and final rows of matrix c contain zeros, with the other rows featuring the pattern [-1 2 -1] along the diagonal. The parameters α_p, α_Q and α_T control the extent of regularization. During the stress computation process, factors such as standard errors and appropriate regularization parameter selection must be taken into account. The stresses P, Q and T are then derived. Finally, the Cartesian stresses are computed as:

$$(\sigma_x)_j = \boldsymbol{P}_j - \boldsymbol{Q}_j \tag{7}$$

$$(\sigma_y)_j = \boldsymbol{P}_j + \boldsymbol{Q}_j \tag{8}$$

$$(t_{xy})_j = \boldsymbol{T}_j \tag{9}$$

In this research, owing to limitations of the strain gauge rosette, digital image correlation (DIC) was utilized to measure displacements and strains, as detailed in the subsequent section. The DIC method is applied to assess displacement fields arising from stress relaxation in the IHD process. This contactless technique has seen substantial advancement in the past twenty years thanks to its notable benefits. It entails taking successive images of the test object's surface prior to and during deformation, followed by analysis using dedicated software to generate comprehensive displacement maps across the entire area. It achieves sub-pixel precision while capturing both planar (2D DIC) and spatial (3D DIC) strains. A high-speed camera that can record fast events accurately is vital for DIC applications, allowing monitoring of material deformation, oscillations, and strains. To facilitate precise point tracking on the surface, a random speckle pattern is commonly applied to the object, creating a distinct texture for the software to follow. The DIC program segments the undeformed (reference) image into smaller subsets, which are then located in the deformed images to compute each subset's movement. By observing shifts in these subsets from the reference to the deformed state, the software determines full-field displacement vectors over the whole surface, offering an in-depth view of the deformation. Based on the displacement data, the software can also derive the strain field through differentiation. This approach employs a continuous polynomial to model the light intensity in each image. Research by Hild and Roux indicated that a fifth-order polynomial provides the best results [23]. The correlation process compares light intensity patterns in selected regions from pre- and post-loading images, evaluating them at the pixel level. The image sub-region that matches the reference most closely is deemed optimal, and the displacement is quantified. To ensure the reliability of each sub-region pair, a correlation coefficient C is defined as [23]:

$$C(R)=\frac{\sum_{i=-m}^{i=m}\sum_{j=-m}^{j=m}\left(G_r(X_P,Y_P)-G_d(X'_P,Y'_P)\right)^2}{\sum_{i=-m}^{i=m}\sum_{j=-m}^{j=m}\left(G_r(X_P,Y_P)\right)^2} \quad (10)$$

$$X_P = x_P + i \quad (11)$$

$$Y_P = y_P + j \quad (12)$$

$$X'_P = x_P + i + U_{s(i,j)} \quad (13)$$

$$Y'_P = y_P + j + V_{s(i,j)} \quad (14)$$

And the description of R is given by:

$$R=\left(X,Y,U,V,\frac{\partial u}{\partial x},\frac{\partial v}{\partial x},\frac{\partial u}{\partial y},\frac{\partial v}{\partial y}\right) \quad (15)$$

Where the parameters are as follows:

U & V: components of displacement

G_r& G_d: functions for interpolating light intensity

(X,Y)&(X',Y'): point coordinates in sub-regions before and after loading, respectively. These are related via:

$$X' = X + U + \frac{\partial U}{\partial x}\Delta x + \frac{\partial U}{\partial y}\Delta y \quad (16)$$

$$Y' = Y + V + \frac{\partial V}{\partial x}\Delta x + \frac{\partial V}{\partial y}\Delta y \quad (17)$$

Where Δx and Δy indicate the distances from the point, respectively. To obtain the solution, C must be minimized, with its gradient set to zero:

$$\nabla C=\left(\frac{\partial C}{\partial R_k}\right)_{k=1,13} \quad (18)$$

The Newton-Raphson method is used to solve Eq. (18).

A schematic representation of the DIC–IHD measurement principle is shown in Fig. 7. Before testing, the specimen surfaces were mechanically polished and coated with a thin layer of matte white paint to obtain a uniform background. A random black speckle pattern was then applied using spray paint to generate a high-contrast texture suitable for DIC tracking.

Image acquisition was performed using a single digital camera (the camera specifications are presented in Table 3) positioned perpendicular to the measurement surface, while an LED light source provided uniform, reflection-free illumination.

Incremental hole drilling was conducted using a 2 mm-diameter drill bit. The hole depth was increased in steps of 0.1 mm (Δh = 0.1 mm) up to a total depth of 2 mm. After each drilling step, the specimen surface was cleaned with compressed air to remove burrs and debris, ensuring clear image capture and reliable strain measurement. The experimental setup used for the DIC–IHD measurements is shown in Fig. 8.

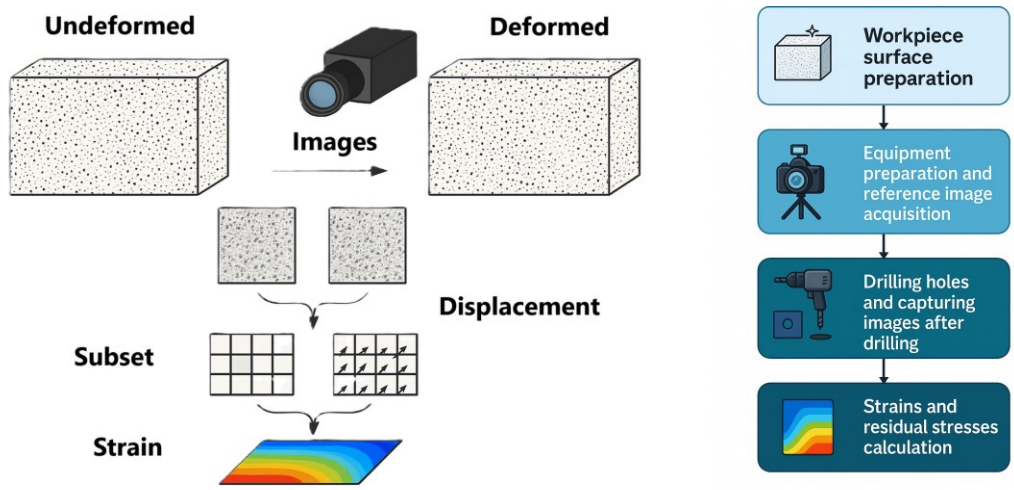

Fig. 7. Schematic illustration of the hybrid DIC–IHD method used for residual stress measurement.

Table 3. Camera configuration for the DIC system

Camera resolution (million)	Lens focal length (mm)	Operating distance (mm)	Horizontal visual field (mm)	Vertical visual field (mm)	Focal length (mm)	Image resolution (pixels)
5	25	250	92	74	120	2592×1944

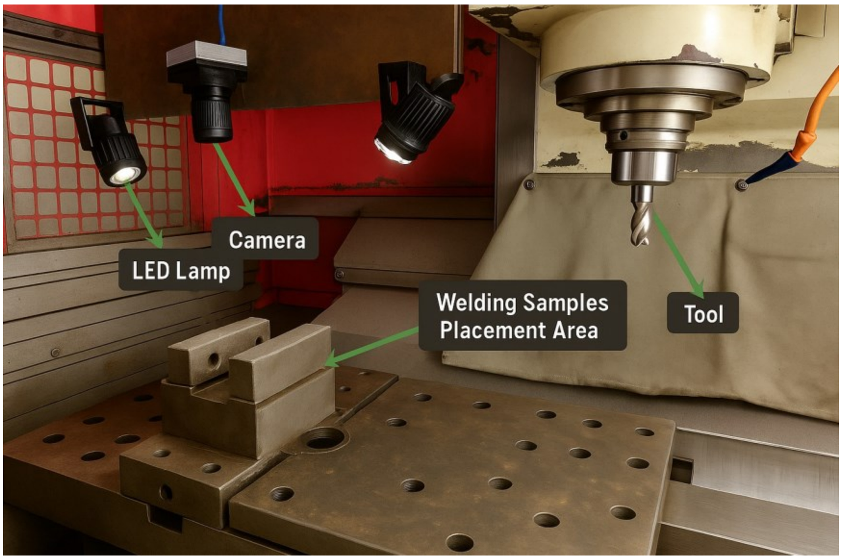

Fig. 8. Experimental setup used for residual stress measurements.

The entire image processing workflow and strain-field calculations were performed using the open-source DIC software Ncorr, an open-source, MATLAB-based digital image correlation platform. Residual stress measurements were taken at a location located on the weld longitudinal centerline and 10 mm below the weld center in the transverse direction. This region was selected to represent the characteristic stress state within the stir and heat-affected zones while minimizing edge effects and disturbances from the tool exit. Incremental strain fields obtained from Ncorr were subsequently converted into in-plane residual stress components using a numerical calibration procedure. The resulting stress–depth curves and interpolated residual stress distributions were later used to compare the influence of different joint angles. Fig. 9 shows the surface preparation and the applied random speckle pattern used for DIC tracking.

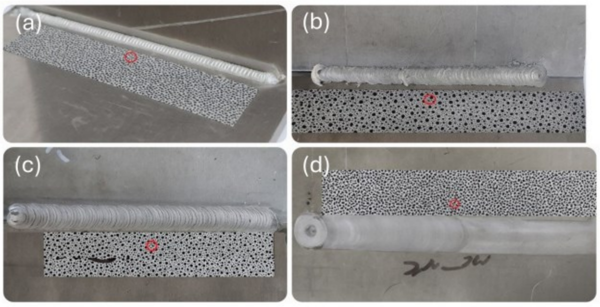

Fig. 9. Specimen surfaces after polishing and speckle pattern application for DIC analysis at joint angles (a) 90°, (b) 150°, (c) 165°, and (d) 180°. The marked regions denote the locations where residual stresses were quantified using the DIC–IHD method.

2.6. Tensile testing

To evaluate the mechanical performance of the friction stir welded joints, tensile tests were carried out for all four joint angles. For the 180° configuration, the welded plates were flat, enabling standard dog-bone specimens to be extracted directly from the weld region in accordance with ASTM E8 without the need for auxiliary fixtures. However, tensile testing of the 90°, 150°, and 165° joints was not feasible with conventional gripping due to the inherent angular geometry of the welded plates. Therefore, custom steel fixtures were designed and fabricated to accommodate each joint angle and to ensure proper load alignment during testing. These fixtures were equipped with threaded holes (M10×1.5) to provide rigid attachment of the angled specimens and to eliminate bending or secondary stress components during loading. The three custom-designed fixtures used to align the angled specimens (90°, 150°, and 165°) during tensile testing are presented in Fig. 10. Their geometry ensured that the loading axis of the universal testing machine remained collinear with the effective tensile axis of the specimens, enabling the joints to be evaluated under pure axial tension. Both the standard dog- bone specimens (for the 180° joint) and the L-shaped specimens (a geometry previously adopted for tensile evaluation of non-planar welds [24]) or angled specimens (for the 90°, 150°, and 165° joints) were prepared using wire-cut electrical discharge machining (EDM) to achieve high dimensional accuracy and avoid thermal distortion.

The tensile test specimens were prepared in five configurations, as summarized in Table 4. For each joint angle, the number of tested specimens was reported to ensure transparency and repeatability of the mechanical evaluation.

All tensile tests were conducted on a Koopa universal testing machine with a maximum load capacity of 20 tons, under identical loading conditions for all joint angles, ensuring a consistent basis for comparing their mechanical responses. Fig. 11 shows the tensile test set up for the different joint-angle configurations.

Fig. 10. Tensile testing fixtures fabricated for the angled FSW configurations: (a) 90°, (b) 150°, and (c) 165°.

Fig. 11. Tensile testing setup showing the specimen mounted inside the wedge grips of the universal testing machine during axial loading.

Table 4. Specifications of the specimens used in the tensile test

Code	Geometry	Joint angle (°)	Weld condition	Manufacturing method	Thickness (mm)	Width (mm)	Number
D-Base	Flat	180	No weld	WireCut- base material	4	6	2
L-90	L-shape	90	Welded	FSW + WireCut	4	40	5
L-150	L-shape	150	Welded	FSW + WireCut	4	40	3
L-165	L-shape	165	Welded	FSW + WireCut	4	40	5
D-Joint	Flat	180	Welded	FSW + WireCut	4	12.5	3

2.7. Microstructural characterization

Microstructural characterization was performed on specimens extracted from the welded region of each joint configuration. For each joint angle, a representative sample was sectioned from the mid-length of the weld using wire electrical discharge machining (EDM), with approximate dimensions of 10 × 10 mm² (full plate thickness). The specimen geometry was selected to be consistent with the corresponding joint angle, ensuring that the weld region remained fully within the observation area. EDM cutting was employed to minimize the introduction of additional thermal or mechanical damage during sectioning.

The extracted specimens were prepared following standard metallographic procedures. Initially, the samples were progressively ground using silicon carbide (SiC) abrasive papers of increasing grit size to remove surface irregularities and achieve a flat surface. The specimens were then mounted in epoxy resin to facilitate handling and improve edge retention during preparation. Final polishing was performed to obtain a smooth, mirror-like surface suitable for microscopic examination. To reveal the weld microstructure, the polished surfaces were chemically etched using Keller's reagent for approximately 5–10 s. The etching time was carefully controlled to ensure proper delineation of grain boundaries without excessive surface attack. After etching, the specimens were rinsed with distilled water and dried prior to observation. Microstructural observations were carried out using a NIM-100 optical microscope to examine the grain morphology and structural characteristics within the weld zone for each joint angle.

2.8. Microhardness measurements

Vickers microhardness measurements were carried out to evaluate the local mechanical response of the welded region for each joint angle. The tests were performed using a microhardness tester under a load of HV0.1 (100 g). The dwell time was selected according to the device's standard operating procedure and maintained within the typical range of 10–15 s to ensure consistent indentation formation.

Hardness measurements were conducted along the thickness direction of the weld cross-section, starting from the top weld surface (0 mm) and progressing toward the mid-thickness of the plate (2 mm), corresponding to half of the 4 mm plate thickness. Indentations were spaced at intervals of 0.4 mm to obtain a detailed hardness profile through the weld depth. For each joint configuration, the resulting hardness values were used to construct depth-dependent hardness profiles, enabling comparison of the microstructural strengthening behavior among different joint angles. The hardness data were later correlated with the residual stress distribution and tensile performance to establish a comprehensive understanding of the thermo-mechanical response of the welded joints.

3. Results and Discussion

3.1. Residual stress results

Residual stress components in both the longitudinal (X-direction, parallel to the weld line) and transverse (Y-direction, perpendicular to the weld line) orientations were obtained using the DIC–IHD method. Fig. 12(a) and 12(b) present the variations of longitudinal (σ_x) and transverse (σ_y) residual stresses, respectively, for the four joint angles investigated (90°, 150°, 165°, and 180°).

In all configurations, the residual stresses were predominantly tensile in both directions, confirming that the FSW process induces plastic stretching during cooling. As seen in Fig. 12 the highest magnitudes of tensile residual stress were recorded for the 90° joint in both σ_x and σ_y components. As the joint angle increased, a consistent reduction in residual stress magnitude was observed, while the tensile nature of the stresses remained unchanged. The longitudinal residual stresses (σ_x) were generally higher than the transverse stresses (σ_y), reflecting the influence of tool motion and material flow direction along the weld line. The reported stress values correspond to the final drilling depth of 2 mm, representing the stabilized residual stress level obtained at the end of the incremental DIC–IHD measurement. Table 5 summarizes the measured residual stress components in both longitudinal (X) and transverse (Y) directions for the four joint angles studied.

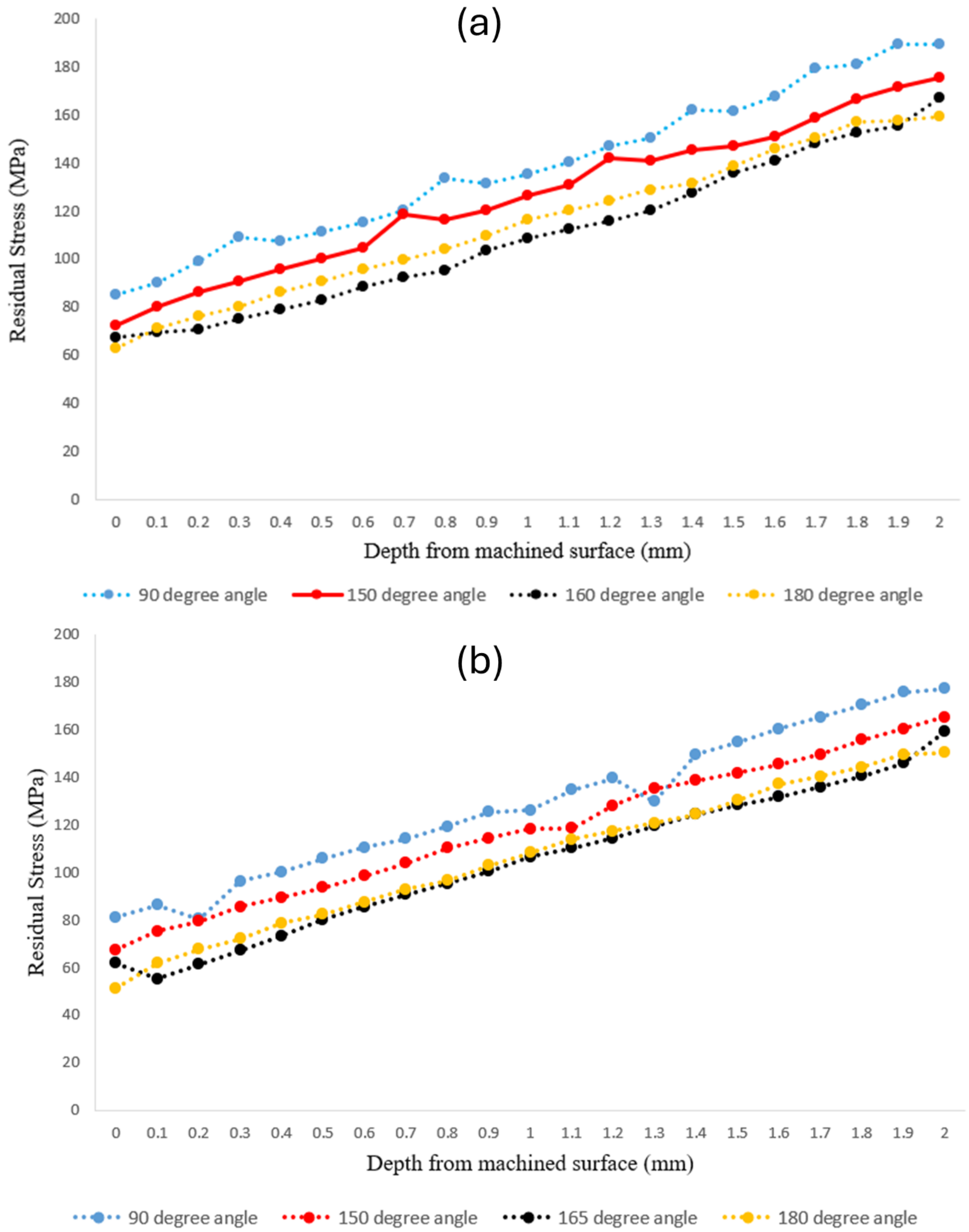

Fig. 12. Residual stress distributions obtained for different joint angles using the DIC– IHD method: (a) longitudinal stress σ_x and (b) transverse stress σ_y.

Table 5. Measured residual stresses in longitudinal (X) and transverse (Y) directions for different joint angles at the final drilling depth of 2 mm.

Joint angle (°)	Longitudinal stress, σx (MPa)	Transverse stress, σy (MPa)
90	189.5	177.3
150	175.3	165.2
165	167.3	159.2
180	159.3	150.3

As seen, the residual stresses are tensile in nature for all configurations. A gradual reduction in stress magnitude is observed as the joint angle increases from 90° to 180°, while the difference between the 165° and 180° joints is minimal. The gradual decrease in both stress components with increasing joint angle can be attributed to a more uniform heat distribution and smoother material flow in larger-angle joints, which reduce thermal gradients and localized plastic strain accumulation. Among the tested configurations, the 165° and 180° joints exhibited very similar and minimal residual stress values, indicating that beyond a certain joint angle, the effect of angle variation on stress generation becomes negligible. Overall, these findings demonstrate that increasing the joint angle mitigates residual stress levels in both directions while maintaining the characteristic tensile nature typical of friction stir welded aluminum joints.

3.2. Microstructural results

Fig. 13 shows the optical microstructures of the weld zone for the four joint configurations (90°, 150°, 165°, and 180°) at 40× and 1000× magnifications. The micrographs indicate that the joint angle has a significant effect on the weld-zone morphology and the overall material flow pattern.

The 90° joint exhibits pronounced directional flow bands at low magnification, indicating asymmetric material transport and localized plastic strain. Based on the optical micrographs, a direct and conclusive grain-scale characterization is not possible. Therefore, any discussion regarding dynamic recrystallization (DRX) or grain refinement should be considered a cautious interpretation rather than direct confirmation from the current observations.

At 150°, the weld-zone morphology becomes more regular and symmetric. This change may be associated with improved material flow and a more balanced thermo-mechanical condition during friction stir welding.

At 165°, the weld zone shows the most uniform and symmetric morphology among all samples. Although the optical images do not provide direct evidence for fully recrystallized equiaxed grains, the overall appearance suggests that this joint configuration provided more favorable thermo-mechanical conditions during welding. This interpretation is also consistent with the mechanical results obtained in the present study, where the 165° specimen exhibited superior performance together with lower residual stress.

At 180°, the weld zone remains relatively uniform; however, some layered features can still be observed. This may indicate that, although the material flow condition was generally acceptable, the thermo-mechanical balance was not as favorable as that observed for the 165° joint.

It should also be noted that some localized defect-like features are visible in certain regions of the weld zone, particularly near the corner areas. These features may be related to local flow instability or insufficient material consolidation under some joint configurations.

Overall, the microstructural characteristics and defect formation observed in friction stir welded aluminum alloys are significantly influenced by the welding process parameters, leading to variations in mechanical properties and residual stress distributions. Previous studies have shown that the development of a fine-grained, dynamically recrystallized microstructure within the weld nugget generally correlates with improved mechanical performance, although parameter optimization is crucial to mitigate defects such as tunnel porosity and worm holes. Similarly, the thermo-

.

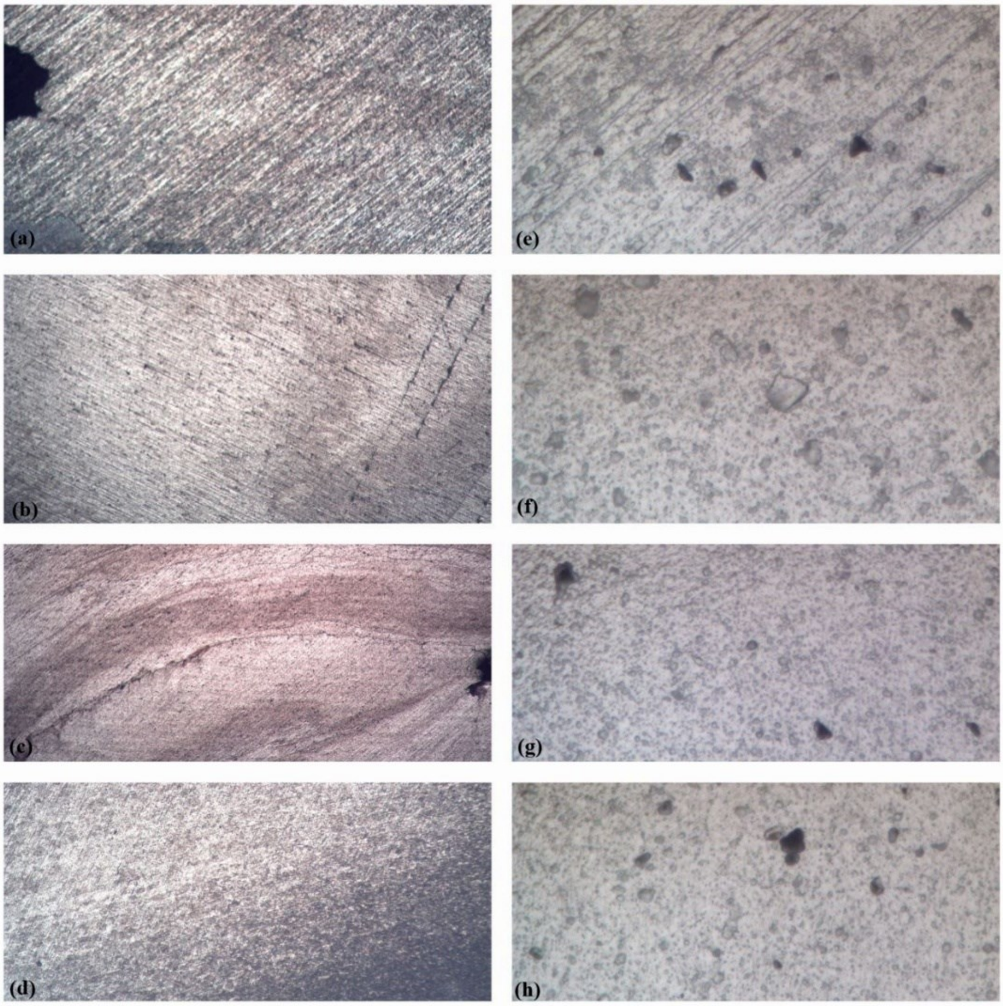

Fig. 13. Optical micrographs of the weld zone for different joint angles: (a-d) 40× magnification showing material flow patterns, and (e-h) 1000× magnification illustrating grain morphology for 90°, 150°, 165°, and 180° configurations.

.

mechanical history inherent to the FSW process profoundly affects the residual stress state, with factors such as material type, joint configuration, and post-weld treatments playing key roles in its magnitude and distribution. Consequently, a comprehensive understanding of these interconnected aspects is vital for ensuring overall weld integrity and quality [25-28].

3.3. Microhardness results

Fig. 14 presents the through-thickness Vickers microhardness (HV0.1) profiles measured from the weld surface (0 mm) to a depth of 2 mm for all joint configurations. The hardness values range approximately between 53 and 65 HV, with distinct depth-dependent trends observed for each angle.

The 90° configuration exhibits the highest near-surface hardness (≈64–65 HV), followed by a noticeable reduction at intermediate depths (≈56–57 HV). The relatively large fluctuation along the thickness indicates heterogeneous plastic deformation and localized strain concentration, which is consistent with the non-uniform microstructure observed for this joint. The 150° joint shows the lowest overall hardness level, with values distributed narrowly around ≈53–57 HV. Although the variation along the depth is moderate, the reduced hardness suggests comparatively limited microstructural refinement within the weld zone.

For the 165° configuration, the hardness profile appears more uniform, with values ranging approximately between 57 and 61 HV and showing minimal gradient through the thickness. This stable distribution reflects homogeneous plastic flow and a more balanced thermo-mechanical condition during welding, supporting the more uniform weld-zone morphology observed in the optical analysis. The 180° configuration demonstrates relatively high hardness near the surface (≈62 HV) followed by a gradual decrease toward mid-thickness (≈55 HV). This trend suggests a surface-dominated strengthening effect associated with localized heat generation and subsequent depth-dependent microstructural evolution. Overall, the hardness results indicate that joint angle significantly influences strain distribution and recrystallization behavior during friction stir welding. Among the investigated configurations, the 165° joint provides the most uniform hardness profile, consistent with its refined microstructure and improved mechanical response.

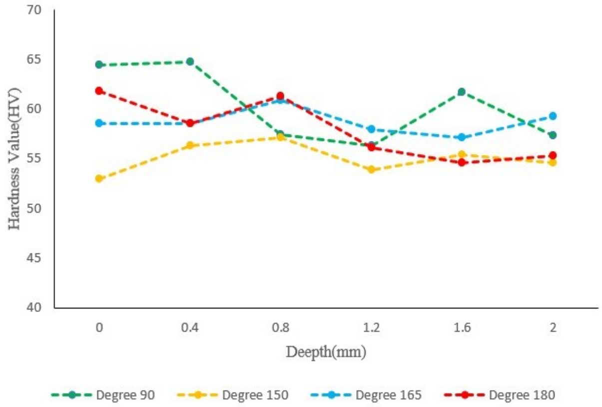

Fig. 14. Through-thickness Vickers microhardness (HV0.1) profiles of friction stir welded AA6061 joints with different joint angles (90°, 150°, 165°, and 180°).

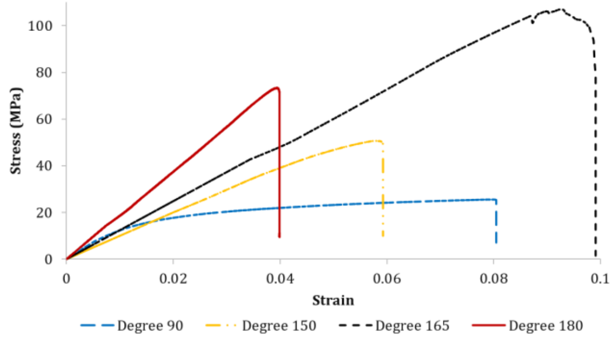

Fig. 15. Comparative engineering stress–strain curves for the four joint configurations.

3.4. Tensile test

Fig. 15 presents the engineering stress–strain curves of the friction stir welded specimens for the four joint angles (90°, 150°, 165°, and 180°). A clear trend is observed in which increasing the joint angle leads to an upward shift of the curves, indicating an improvement in the load-bearing capacity of the welded joints.

The 90° specimen exhibited the lowest tensile strength, with its curve terminating at comparatively small stress values, which can be attributed to the severe geometric discontinuity that induces localized stress concentration and disrupts uniform plastic material flow during the FSW process. However, this configuration showed a relatively higher strain to failure compared with the 150° and 180° joints, which may be associated with the deformation characteristics of the L-shaped geometry allowing greater global displacement before final fracture.

The specimen welded at 150° demonstrated higher strength than the 90° configuration, reflecting enhanced material flow and improved structural continuity along the weld line, as the less restrictive joint geometry facilitates more stable material mixing and consolidation within the stir zone.

A significant improvement was observed at 165°, where the stress–strain curve becomes noticeably taller and more elongated. This joint angle achieved the highest yield strength, ultimate tensile strength, and fracture strain among all tested configurations, indicating that the 165° joint provides the most favorable combination of strength and ductility. This finding suggests that this angle establishes an optimal balance between tool-induced plastic deformation, heat input, and lateral material flow, thereby minimizing internal defects and promoting a more homogeneous weld-zone morphology.

Although the 180° joint also exhibited high tensile strength, its performance remained slightly below that of the 165° specimen, which may be related to differences in localized heat distribution and cooling behavior between the flat and angled configurations, affecting microstructural evolution.

To provide an overall comparison of the tensile behavior at different joint angles, Fig. 16 and Table 6 summarize the yield, ultimate, and failure stresses for all configurations. Overall, the results confirm that increasing the joint angle from 90° to 180° generally enhances the mechanical performance of friction stir welded AA6061 aluminum, with the 165° configuration exhibiting the most balanced combination of strength and ductility due to improved weld consolidation and microstructural uniformity.

3.5. Integrated correlation of microstructural and mechanical responses

The experimental findings demonstrate a clear interrelationship between joint angle, microstructural evolution, hardness distribution, residual stress development, and tensile performance. Rather than acting as an isolated geometric parameter, the joint angle fundamentally governs the thermo-mechanical conditions during friction stir welding, thereby controlling the overall mechanical response of the weld. In the 90° configuration, asymmetric material flow and localized strain concentration resulted in a non-uniform weld-zone morphology and pronounced hardness fluctuation through the thickness. This non-uniform deformation behavior intensified residual stress accumulation and contributed to premature tensile failure. The combination of microstructural non-uniformity and elevated tensile residual stresses explains the inferior mechanical performance observed for this condition. Increasing the joint angle to 150° partially improved material flow regularity and grain refinement. Although hardness variation was reduced compared to the 90° joint, the thermo-mechanical balance was still not fully optimized, limiting the enhancement in tensile properties. The 165° configuration provided the most favorable integrated response. Symmetric material flow provided more promoted a more complete dynamic recrystallization process, resulting in a relatively uniform hardness profile and a more uniform weld-zone morphology. The homogeneous strain distribution reduced residual stress concentration, allowing more stable plastic deformation during tensile loading. This balanced microstructural and mechanical state explains the superior strength and ductility measured for the 165° joint. Although the 180° joint exhibited relatively low residual stress levels, slight structural layering and a depth-dependent hardness gradient indicate that complete flattening does not maximize strain uniformity to the same extent as the 165° configuration. This suggests the existence of an optimal geometric range in which thermo-mechanical coupling is most effective.

Overall, the results confirm that joint angle dictates material flow symmetry, recrystallization behavior, hardness uniformity, and residual stress evolution, which collectively determine the tensile performance of friction stir welded AA6061 joints. Among the investigated configurations, the 165° angle represents the most balanced and mechanically efficient condition.

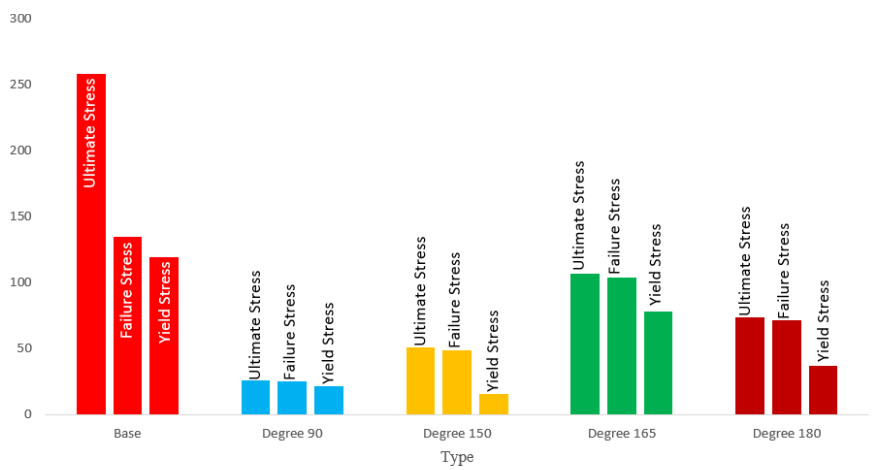

Fig. 16. Summary of tensile strength metrics (yield, ultimate, and failure stresses) for the base material and the welded joints. A pronounced improvement in tensile capacity is observed as the joint angle increases from 90° to 165°, after which, a slight reduction is noted at 180°, confirming the optimal performance at 165°.

Table 6. Tensile properties of the base material and FSW joints at different joint angles

Property	Base	90°	150°	165°	180°
Yield stress (MPa)	119.6	21.8	15.44	77.9	36.7
Fracture stress (MPa)	134.5	25.0	49.0	104.2	71.37
Ultimate tensile strength (MPa)	258.0	25.54	50.7	107.0	73.4

4. Conclusions

This study systematically investigated the influence of joint angle on the thermo-mechanical response of friction stir welded AA6061 joints. The main findings are summarized as follows:

• Tensile residual stresses decreased progressively with increasing joint angle, from approximately 189.5 MPa (σx) at 90° to 159.3 MPa at 180°, confirming the strong influence of joint geometry on stress evolution.

• Microstructural observations, primarily from optical microscopy, indicated improvements in material flow symmetry with increasing joint angle. The resulting microstructure in the 165° configuration appeared more homogeneous compared to other angles, which is consistent with findings in the literature suggesting that such configurations can promote more favorable conditions for dynamic recrystallization and grain refinement in friction stir welding.

• The through-thickness microhardness values ranged between approximately 53 and 65 HV0.1, with the 165° joint showing the most uniform hardness distribution, reflecting balanced thermo-mechanical conditions.

• Tensile testing demonstrated a substantial improvement in mechanical performance with increasing joint angle, with the 165° configuration achieving the highest ultimate tensile strength (≈107 MPa) compared to ≈25 MPa at 90°.

• Although the 180° joint exhibited slightly lower residual stress levels, its tensile performance did not exceed that of the 165° configuration, indicating the existence of an optimal geometric range rather than a monotonic improvement with increasing angle.

Overall, the results confirm that joint angle governs material flow symmetry, recrystallization behavior, residual stress development, and mechanical performance. Among the investigated configurations, the 165° configuration provides the most favorable integrated thermo-mechanical condition.

Author’s contributions

F. AghaAbdollahian: Writing -original draft, Software, Resources, Investigation, Formal analysis, Data curation, Conceptualization

M. Honarpisheh: Writing- review & editing, Visualization, Supervision, Project administration, Methodology, Funding, acquisition

Competing interests

The authors declare that they have no known competing financial interests or personal relationships that could have appeared to influence the work reported in this paper.

Funding

The authors declare that no funds were received during the preparation of this manuscript.

5. References

[1] Shah, P. H., & Badheka, V. J. (2019). Friction stir welding of aluminium alloys: An overview of experimental findings–Process, variables, development and applications. *Proceedings of the Institution of Mechanical Engineers, Part L: Journal of Materials: Design and Applications*, *233*(6), 1191-1226. https://doi.org/10.1177/1464420716689588

[2] Mishra, R. S., & Ma, Z. Y. (2005). Friction stir welding and processing. *Materials Science and Engineering: R: Reports, 50*, 1-78. https://doi.org/10.1016/j.mser.2005.07.001

[3] Lohwasser, Daniela, and Zhan Chen, eds. *Friction stir welding: From basics to applications*. Elsevier, 2009.

[4] Robi, P. S., Pal, S., & Parida, B. (2018). 22 Recent trends and advances in friction stir welding and friction stir processing of metals.

[5] Beygi, R., Zarezadeh Mehrizi, M., Akhavan-Safar, A., Mohammadi, S., & da Silva, L. F. (2023). A parametric study on the effect of FSW parameters and the tool geometry on the tensile strength of AA2024–AA7075 joints: microstructure and fracture. *Lubricants*, *11(2)*, 59. https://doi.org/10.3390/lubricants11020059

[6] Prodkornburee, T., & Uthaisangsuk, V. (2025). Modeling of tensile properties and failure of friction stir welded dissimilar aluminum alloys coupled with process-induced defects. *The International Journal of Advanced Manufacturing Technology*, *136*(7), 3263-3284. https://doi.org/10.1007/s00170-025-15001-3

[7] Thilagham, K.T., & Noorullah, D. (2025). Aluminum alloys based on response surface methodology optimization and categorization of FSW for AA7075 & AA6082. *Smart Science, 13*, 1-15. https://doi.org/10.1080/23080477.2024.2445319

[8] Garcia Ruano, S. A., Delijaicov, S., & dos Santos Junior, A. A. (2023). Acoustoelasticity to measure residual stresses in plates of 5052 aluminum joined by FSW. *Journal of the Brazilian Society of Mechanical Sciences and Engineering*, *45*(2), 82. https://doi.org/10.1007/s40430-022-03998-7

[9] Vahidshad, Y., Rasfijani, A., & Abbasi, A. (2025). The effect of FSW parameters on residual stresses in aluminum alloy using finite element analysis. *Space Science, Technology and Applications*, e229773. https://doi.org/10.22034/jssta.2025.506404.1232

[10] Salvati, E., Everaerts, J., Kageyama, K., & Korsunsky, A. M. (2019). Transverse fatigue behaviour and residual stress analyses of double sided FSW aluminium alloy joints. *Fatigue & Fracture of Engineering Materials & Structures*, *42(9)*, 1980-1990. https://doi.org/10.1111/ffe.13068

[11] Yaowu, X. U., & Rui, B. A. O. (2017). Residual stress determination in friction stir butt welded joints using a digital image correlation-aided slitting technique. *Chinese Journal of Aeronautics*, *30(3)*, 1258-1269. https://doi.org/10.1016/j.cja.2016.11.003

[12] Chatterjee, A., Mandal, A., & Giri, A. (2024). A study on residual stress measurement by DIC approach in FSW welded AA6082 joints. *Procedia Structural Integrity*, *60*, 13-19. https://doi.org/10.1016/j.prostr.2024.05.027

[13] Manikandan, R., Elatharasan, G., Parthiban, A., Sakthivel, T. G., Gopalakrishnan, T., & Raju, R. (2025). Experimental and computational analysis of thermal and mechanical characteristics in friction stir welding of dissimilar aluminum alloys with varying tool pin geometries. *Welding in the World*, *69(7)*, 2003-2029. https://doi.org/10.1007/s40194-025-01975-x

[14] Zhang, Y., Shi, J., Liao, G., Li, R., Peng, J., Kuang, S., & Shen, F. (2025). Effects of tool structure and process parameters in friction stir welding on the temperature and mechanical properties of dissimilar copper–aluminium welded joints. *Metals, 15(2)*, 193. https://doi.org/10.3390/met15020193

[15] Beygi, R., Talkhabi, A. A., Mehrizi, M. Z., Marques, E. A., Carbas, R. J., & da Silva, L. F. (2023). A novel Lap-Butt joint design for FSW of aluminum to steel in tee-configuration: joining mechanism, intermetallic formation, and fracture behavior. *Metals*, *13(6)*, 1027. https://doi.org/10.3390/met13061027

[16] Seleman, M. M. E. S., Ahmed, M. M. Z., Ramadan, R. M., & Zaki, B. A. (2022). Effect of FSW parameters on the microstructure and mechanical properties of T-joints between dissimilar Al-alloys. *International Journal of Integrated Engineering, 14*(1), 1-12. https://doi.org/10.30880/ijie.2022.14.01.001

[17] Liu, S., Chen, F., & Gao, Y. (2025). Effect of Progressive Pin and Pre-set Wires on the Quality of Corner Forming of Al/Cu FSW T-Lap Joints. *Journal of Materials Engineering and Performance, 34*(15), 15774-15786. https://doi.org/10.1007/s11665-024-10278-z

[18] Jamshidi Aval, H., Serajzadeh, S., & Kokabi, A. H. (2012). Experimental and theoretical evaluations of thermal histories and residual stresses in dissimilar friction stir welding of AA5086-AA6061. *The International Journal of Advanced Manufacturing Technology, 61*(1), 149-160. https://doi.org/10.1007/s00170-011-3713-8

[19] Astm, E. (2013). 837-13a standard test method for determining residual stresses by the hole-drilling strain-gage method. *ASTM International, West Conshohocken*.

[20] Buffa, G., Hua, J., Shivpuri, R., & Fratini, L. (2006). Design of the friction stir welding tool using the continuum based FEM model. *Materials Science and Engineering: A, 419*(1-2), 381-388. https://doi.org/10.1016/j.msea.2005.09.041

[21] Mohd Yasin, M. N. F. (2013). Study on strength of friction stir welded plate in corner joint configuration.

[22] Davis, J. R. (1993). *Aluminum and aluminum alloys*. ASM international.

[23] Hild, F., & Roux, S. (2012). Digital image correlation. *Optical methods for solid mechanics. A full-field approach*, *367*, 183-228.

[24] Setiawan, W., Darmadi, D. B., Suprapto, W., Soenoko, R., & Gunawan Tri, S. (2019). Varied corner joint design aluminium 6061 using friction stir welding. *IOP Conference Series: Materials Science and Engineering*, *494*(1), 012106. https://doi.org/10.1088/1757-899X/494/1/012106

[25] Mohammadzadeh Jamalian, H., Farahani, M., Besharati Givi, M. K., & Aghaei Vafaei, M. (2016). Study on the effects of friction stir welding process parameters on the microstructure and mechanical properties of 5086-H34 aluminum welded joints. *The International Journal of Advanced Manufacturing Technology*, *83*(1), 611-621. https://doi.org/10.1007/s00170-015-7581-5

[26] Abankar, M., Lunetto, V., De Maddis, M., & Russo Spena, P. (2024). Friction stir welding of additively manufactured A20X aluminum alloy: welding process, mechanical properties, and microstructure. *The*

International Journal of Advanced Manufacturing Technology, 135(9), 4635-4652. https://doi.org/10.1007/s00170-024-14747-6

[27] Liu, X., Xie, P., Wimpory, R., Li, W., Lai, R., Li, M., Chen, D., Liu, Y., & Zhao, H. (2019). Residual stress, microstructure and mechanical properties in thick 6005A-T6 aluminium alloy friction stir welds. *Metals*, *9*(7), 803. https://doi.org/10.3390/met9070803

[28] Reddy, G. M., Mastanaiah, P., Murthy, C. V. S., Mohandas, T., & Viswanathan, N. (2006, December). Microstructure, residual stress distribution and mechanical properties of friction-stir AA 6061 aluminium alloy weldments. In *Indian Society for Non-Destructive Testing, Hyderabad Chapter, Proc. National Seminar on Non-Destructive Evaluation*.